IEEE Robotics and Automation Letters (RAL) paper presented at
2024 IEEE/RSJ International Conference on Intelligent Robots and Systems (IROS)
October 14-18, 2024. Abu Dhabi, UAE

Optimal Design of Linkage-Driven Underactuated Manipulator for Precise Pinching and Powerful Grasping

Meng Hailiang, Yang Kaiyu, Zhou Lingxuan, Shi Yixiao, Cai Shibo, Bao Guanjun, *Member, IEEE*

***Abstract*— Pinching and grasping are the key fundamental actions for manipulator to handle objects, and achieving high-quality execution of these actions has always been an intense attention in robotics field. In this paper, a novel underactuated manipulator with composed multiple-linkage mechanism is proposed, which enables both precise pinching and powerful grasping functions. To eliminate trajectory errors of linear pinching, the linkage mechanism is optimized by genetic algorithm based on modelling and kinematic analysis of the finger. The optimized configuration results in a vertical displacement error less than 0.3mm and a linear deviation less than 1%. Furthermore, the envelope linkage mechanism is optimized by taking the uniformity of force distribution, which is chosen as a performance indicator. Additionally, a rotary mechanism is installed at the proximal interphalangeal of the finger to enable the manipulator to switch different grasping modes for various types of objects. Finally, the experiments on pinching small and thin objects and grasping objects with pose-varied mode demonstrate that the developed manipulator is capable of both precise pinching and powerful grasping. This work offers a promising solution for the robotic manipulator to perform multi-type object grasping tasks.**

***Index Terms*— Multi-finger manipulator, Underactuated mechanism, Linkage mechanism, Linear pinching, Envelope Grasping.**

I. Introduction

The most frequently used actions in human daily life are powerful grasp and precise pinch [1], which means that these two actions fulfill the requirements for using most objects in daily life. The same applies to robotic hands. On one hand, it requires that manipulators should be designed with the multi-fingered configuration (more than three fingers). On the other hand, it also requires that manipulators possess both enveloping grasp and pinch capabilities, especially in the pinching function. The fingertips should be able to move in parallel for grasping small objects on a flat surface. However, it is challenging to directly apply mechanical structures to provide manipulator with powerful grasping and precise pinching capabilities.

Multi-fingered robotic hands have attracted intensive attention due to their ability to flexibly and accurately manipulate diverse objects. According to the configuration of the actuator and the degrees of freedom (DOF) of mechanism, robotic hands can be classified into two types: fully actuated [2] and underactuated [3]. Fully actuated means that each joint is powered by an actuator and can move independently, which can achieve precise motion control and high flexibility [4]. However, these kinds of hands have drawbacks such as complex structure, difficulty in control, and high cost. Underactuated means that the number of actuators is less than its DOF. This type of structure is more reliable, cost-effective, and easier to control compared to fully actuated hands due to the simplified actuation and transmission [5]. Therefore, underactuated structures are believed to have wider application prospects in robotic grasping tasks [6].

The transmission modes of underactuated manipulators include gear [7], tendon-driven [8] and linkage-driven [9,10] mechanisms. Tendon-driven designs offer a compact size and the joint motion characteristics, which can be adjusted by using tendons with different winding paths [11-14]. However, it is difficult to establish an accurate mathematical model for tendon-driven mechanisms [15-16]. Furthermore, the transmission efficiency is low, and there is uneven force distribution during grasping. In contrast, linkage-driven mechanisms are simpler, more reliable, and have higher transmission efficiency, allowing for greater gripping force [17], which is particularly attractive for prosthetic hand designs [18,19]. Several underactuated robotic hands have been designed using linkage mechanisms. Kim et al. [20] proposed a dexterous robot hand with biomimetic mechanism, and the finger is driven by four-coupled link mechanism with two linear actuators. Panipat et al. [21] designed a five-fingered prosthetic hand that has multiple grip patterns with the use of only one actuator, the different move patterns are achieved through the use of multiple sets of rigid four-bar linkages, and Wu et al. [22] designed the fully rotational three-fingered hand based on the coupling grasping principle. Other examples include the pneumatically-driven linkage-driven hand developed by Begoc et al. [23], the uGRIPP three-fingered robotic hand developed by Yamaguchi et al. [24], and the underactuated manipulator based on the metamorphic mechanism principle designed by Sun et al [25]. Although these underactuated robotic hands can perform powerful and stable grasping and holding tasks, it is difficult for them to grasp small and thin objects placed on the workbench. To solve this problem, Luo et al. [26] added linear actuators to the proximal finger joints to offer linear motion of the fingertips, and designed a two-fingered robotic hand VGS with a hybrid gripping mode. Li et al. [27] also proposed a linear adaptive mechanical gripper with a four-bar sliding base to compensate for finger-end displacement. Watanabe et al. [28] further designed a gripper based on a six-bar linkage mechanism that can perform parallel and

*Research supported by the Key Research and Development Program of Zhejiang (Grand No. 2021C04015), the Zhejiang Provincial Natural Science Foundation of China (Grand No. LZ23E050005). (Corresponding author: gjbao@zjut.edu.cn).

The authors are with the College of Mechanical Engineering, Zhejiang University of Technology, Hangzhou 310023 China, and also with the Key Laboratory of Special Purpose Equipment and Advanced Processing Technology, Ministry of Education and Zhejiang Province, Zhejiang University of Technology, Hangzhou 310023, China (e-mail: gjbao@zjut.edu.cn).

Preprint submitted to IEEE Robotics and Automation Letters as Submission for RA-L only
Received October 31, 2023 09:04:03 Pacific Time

flipping grasping. Nevertheless, Zheng et al. [29] fixed an eccentric cam to the four-bar linkage mechanism of the finger to compensate the finger-end height and perform linear parallel grasping.

However, owing to the limitation of mechanical structures, the trajectory of the distal interphalangeal joint (DIP) of existing linkage-driven manipulators is usually arc-shaped, resulting in displacement in the longitudinal direction, as shown in Fig. 1(a). Without displacement compensation algorithms or external assistance, it is difficult for the manipulator itself to grasp small or thin objects. Watanabe et al' s manipulator [28] is able to grasp small objects without the need for such compensation, but it is not able to grasp larger objects with an enveloping grasp since it only has two fingers.

Therefore, we proposed a composed multiple-linkage mechanism (shown in Fig. 1(b)) to construct an underactuated robotic finger with precise pinching and powerful grasping abilities. The DIP undergoes translation in the pinching mode as shown in Fig. 1(c), and after contact with an object, the proximal interphalangeal joint (PIP) and middle interphalangeal joint (MIP) have no relative motion, which can be regarded as a two-joint structure. If the MIP or PIP contacts an object before the DIP, the finger will switch to enveloping mode and perform powerful grasping, which can be regarded as a three-joint structure. The proposed finger will enable underactuated robotic hands to work in multiple modes for diverse grasping tasks.

II. Structure and Optimal Design

A. The structure of underactuated manipulator

According to the proposed composed multiple-linkage mechanism, the three-finger underactuated manipulator is designed as shown in Fig. 2, which has three typical working

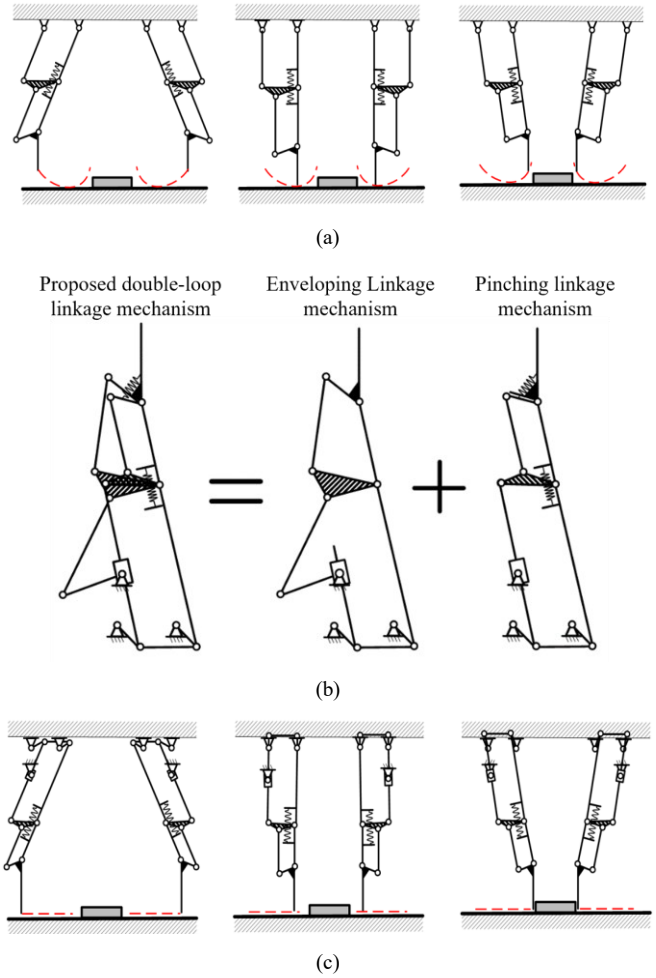

Fig. 1. Diagram of manipulator. (a) Traditional pinching, (b) proposed pinching, (c) composed multiple-linkage mechanism.

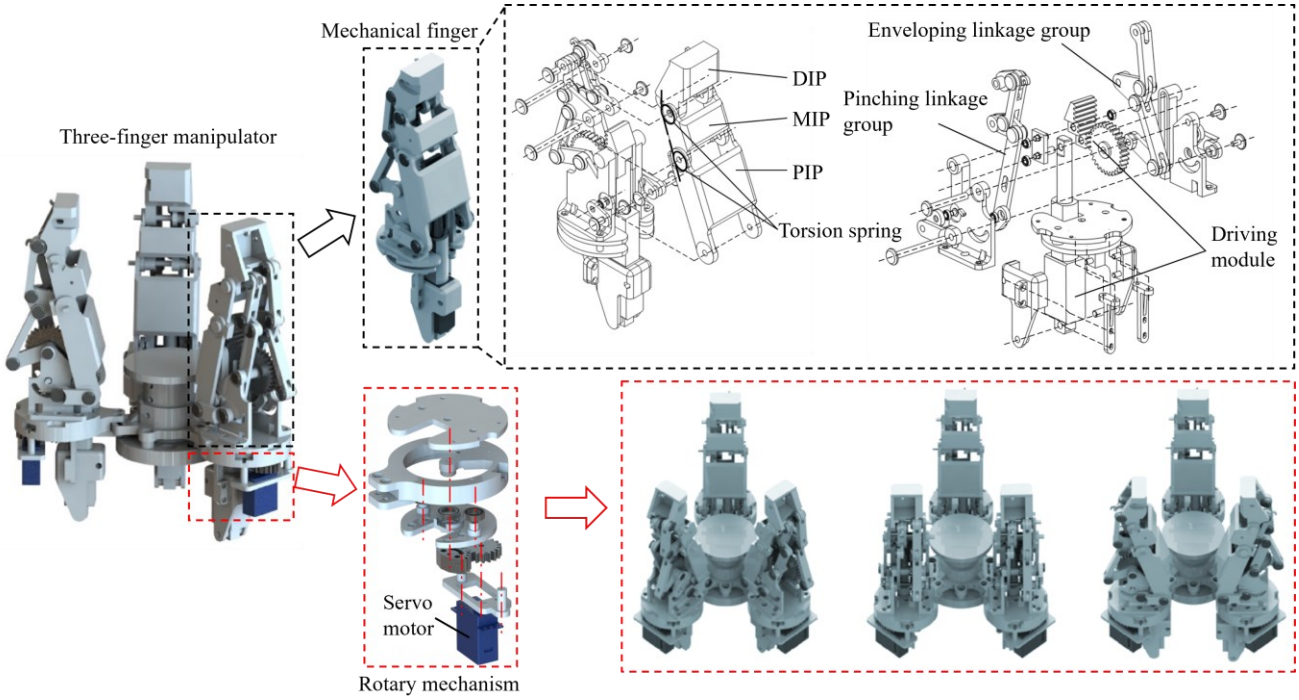

Fig. 2. The structure of underactuated manipulator.

modes, including three-finger centering grasping, three-finger parallel grasping, and two-finger symmetrical pinching. The developed underactuated finger mainly consists of a pinching linkage group, an enveloping linkage group, and a driving module. The pinching linkage group is used to enable the translational motion of the fingertip. The function of the enveloping linkage group is to endow the mechanical finger with powerful grasping ability. The driving module consists of a linear motor and a gear mechanism, providing torque to the robotic finger. The three finger joints are used to connect the two sets of linkage groups. There are torsion springs installed between the finger joints so that the PIP and MIP do not rotate relative to each other without contacting with any target, and the DIP will perform a translational motion. Conversely, the driving torque overcomes the constraint force of the torsion spring between the finger joints, resulting in an enveloping motion. In order to enable the underactuated robotic hand to switch finger configurations and adopt different types of grasping modes based on the shape of objects, as shown in the lower right of Fig. 2, we designed a rotary mechanism, which is driven by the servo motor. This rotary mechanism allowing the fingers to have a 90° repositioning freedom relative to the palm.

The ratio of human finger bones length is approximately 1:1:2 [30] and the length of the middle finger of a normal adult is about 120mm.The assembly size of the designed underactuated finger is shown in Fig. 3(a). Based on the features of human fingers and fine-tuning in the design process, we have set the lengths of the mechanical fingers as 38mm, 30mm, and 63mm, respectively. The ranges of joint motion are measured by using SolidWorks as 0-73°, 0-62°, and 0-44°, respectively. The finger has two working modes: translational motion as shown in Fig. 3(b) and enveloping motion as shown in Fig. 3(c).

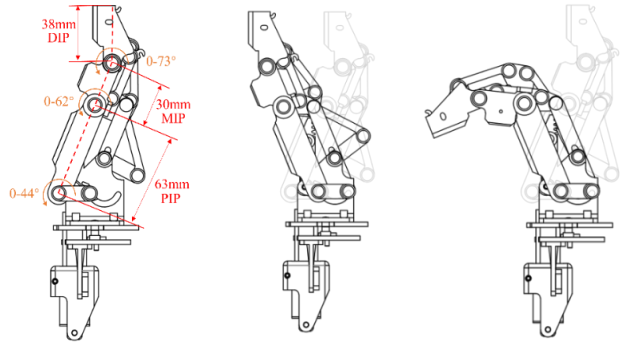

(a) (b) (c)

Fig. 3. Mechanical structure of the finger. (a) The size of the joints, (b) translational motion, (c) enveloping motion.

B. *The optimization of pinching linkage group*

An inverted slider-crank linear guiding mechanism is used for the pinching linkage group. As shown in Fig. 4(a), AB is the driving rod. With the constraint of the elastic element, FE and EC rods remain collinear and the angle between GF and HF rods remains constant. The GF rod (DIP) can keep vertical motion by setting the angle between GF and HF. The linear guiding mechanism consists of AB rod, BJ rod, FE rod, and K slider, where BJ and FE can be regarded as a whole. Therefore, the mechanism can be simplified as shown in Fig. 4(b).

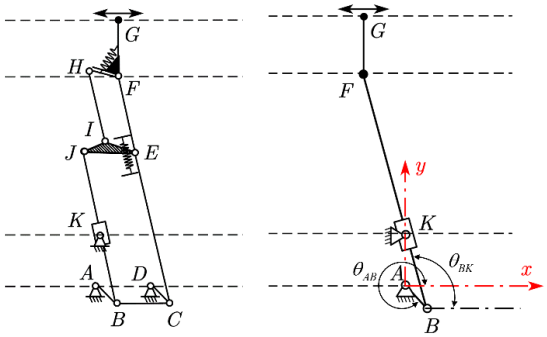

(a) (b)

Fig. 4. Inverted slider-crank linear guiding mechanism. (a) Diagram, (b) equivalent diagram.

From the geometric relationship in Fig. 4(b), the coordinate of $K(x_K,y_K)$ can be calculated as:

$$\begin{cases} x_K = l_{AB}\cos(\theta_{AB}) + l_{BK}\cos(\theta_{BK}) \\ y_K = l_{AB}\sin(\theta_{AB}) + l_{BK}\sin(\theta_{BK}) \end{cases} \tag{1}$$

After transforming the equation (1), square both sides of the equation, as:

$$\begin{cases} (x_K - l_{AB}\cos(\theta_{AB}))^2 = (l_{BK})^2\cos^2(\theta_{BK}) \\ (y_K - l_{AB}\sin(\theta_{AB}))^2 = (l_{BK})^2\sin^2(\theta_{BK}) \end{cases} \tag{2}$$

Then, eliminating θ_{BK} as:

$$l_{BK}^2 = x_K^2 + y_K^2 + l_{AB}^2 - 2x_K l_{AB}\cos(\theta_{AB}) - 2y_K l_{AB}\sin(\theta_{AB}) \tag{3}$$

Based on the cosine theorem, it can be obtained as:

$$\begin{cases} \cos(\angle ABK) = \dfrac{l_{AB}^2 + l_{BK}^2 - l_{AK}^2}{2l_{BK}l_{AB}} \\ \cos(\angle BKA) = \dfrac{l_{BK}^2 + l_{KA}^2 - l_{AB}^2}{2l_{BK}l_{KA}} \end{cases} \tag{4}$$

Based on geometric relationships and equation (3) to (4), the coordinate of $F(x_F,y_F)$ can be calculated as:

$$\begin{cases} x_F = \begin{cases} l_{AB}\cos(\theta_{AB}) + l_{BF}\sin(\angle BKA) & 0(\dfrac{3\pi}{2}) \le \theta_{AB} < \dfrac{\pi}{2}(2\pi) \\ l_{AB}\cos(\theta_{AB}) - l_{BF}\sin(\angle BKA) & \dfrac{\pi}{2} \le \theta_{AB} < \dfrac{3\pi}{2} \end{cases} \\ y_F = l_{KF}\cos(\angle BKA) - l_{AB}\cos(\angle ABK + \angle BKA) \end{cases} \tag{5}$$

In order to further reduce the linear error of the DIP trajectory by optimizing the rod length of the equivalent inverted slider-crank mechanism. We select 10 equidistant points on the trajectory of point F, and take the average of y_{Fi} (i=1~10) as y_{Fa}. The line trajectory tracking error is defined as:

$$f = \sum_{i=1}^{10}(y_{Fi} - y_{Fa})^2 \tag{6}$$

The translation range of the manipulator is set to 0-100 mm, so the mechanical finger has a translational 50 mm motion range. The optimization of the rod length is carried out with the linear trajectory tracking error as the objective function. The l_{AB}, l_{AK}, and l_{BF} are constrained separately to {[8,12], [16,24], [90,100]}, and optimized by using

MATLAB genetic algorithm toolbox (with default parameter settings). After that, the l_{AB}, l_{AK}, and l_{BF} are estimated respectively as 10.069, 20.046, and 93.168, which can be rounded to 10, 20, and 93. The variation curve of F (x_F, y_F) with respect to θ_{AB} can be obtained by substituting x_K=0, y_K=20 mm, l_{AK}=20 mm, and l_{BF}=93 mm into (3), as shown in Fig. 5. It can be observed from Fig. 5(a) that y_F remains almost constant within the range of 180°≤θ_{AB}≤360°.Based on translation range of the finger (50mm, that is x_F∈[-25, 25]), the range of θ_{AB} can be set to [200.5°, 349.5°], and y_F remains at about 83 mm. Fig. 5(b) shows the movement trajectory of F obtained through MATLAB simulation, which indicates that the longitudinal displacement of the DIP is about 0.13 mm, the lateral displacement is 50 mm, and the linear deviation is 0.26% during the translational motion.

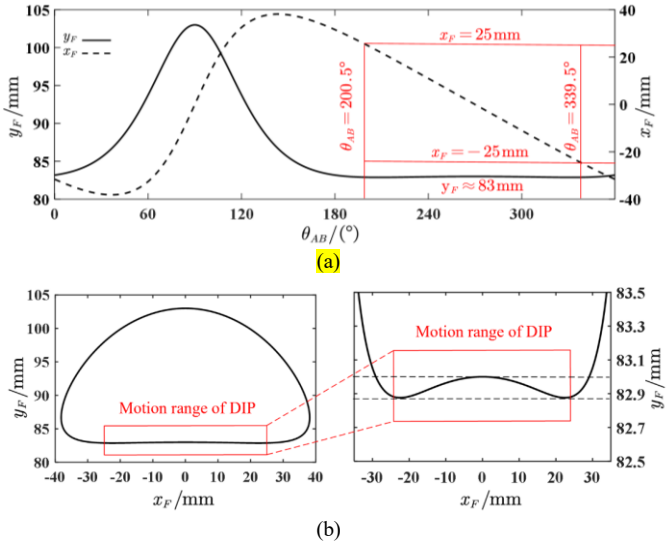

Fig. 5. Kinematic profile of point F. (a) Displacement with respect to θ_1, (b) trajectory.

C. The optimization of enveloping linkage group

The rod length of enveloping linkage group can be optimized by using the statics model of the envelope motion. As shown in Fig. 6(a), the driving torque is T_0, and the points that the three finger joints contact with the object are respectively P_1, P_2, and P_3, and the reaction forces are respectively F_1, F_2, and F_3.

The gravitational force of the finger and the friction between the finger and the object are ignored. According to the principle of virtual work, it can be derived that:

$$\boldsymbol{T}^T\boldsymbol{\omega}=\boldsymbol{F}^T\boldsymbol{V} \tag{7}$$

where $\boldsymbol{T}$ is the input torque vector; $\boldsymbol{\omega}$ represents the angular velocity vector; $\boldsymbol{F}$ represents the reaction forces applied to the three finger joints; $\boldsymbol{V}$ represents the velocity vector.

There exists a Jacobian matrix $\boldsymbol{J}_V$, such that the velocity vector $\boldsymbol{V}$ and the angular velocity vector $\dot{\boldsymbol{\theta}}$ satisfy the following relationship:

$$\boldsymbol{V}=\boldsymbol{J}_V\dot{\boldsymbol{\theta}} \tag{8}$$

The transformation matrix $\boldsymbol{J}_\omega$ is

$$\dot{\boldsymbol{\theta}}=\begin{bmatrix}\dot{\theta}_1 & \dot{\theta}_2 & \dot{\theta}_3\end{bmatrix}^T=\boldsymbol{J}_\omega\boldsymbol{\omega} \tag{9}$$

From (7)-(9), it has:

$$\boldsymbol{F}=(\boldsymbol{J}_V^{-1})^T(\boldsymbol{J}_\omega^{-1})^T\boldsymbol{T} \tag{10}$$

The expression of grasping force can be obtained by calculating $\boldsymbol{J}_V$ and $\boldsymbol{J}_\omega$. The calculation of $\boldsymbol{J}_V$ can be derived from (11), and the detailed derivation process can be found in reference [24].

$$\begin{bmatrix}\boldsymbol{F}_1 & \boldsymbol{F}_2 & \boldsymbol{F}_3\end{bmatrix}\begin{bmatrix}\partial\boldsymbol{P}_1\\ \partial\boldsymbol{P}_2\\ \partial\boldsymbol{P}_3\end{bmatrix}=\begin{bmatrix}F_1 & F_2 & F_3\end{bmatrix}\boldsymbol{J}_V\begin{bmatrix}\dot{\theta}_1\\ \dot{\theta}_2\\ \dot{\theta}_3\end{bmatrix} \tag{11}$$

The solution of $\boldsymbol{J}_\omega$, as shown in Fig. 6(b), the angular velocity relationship can be obtained through instantaneous center theory based on the velocity analysis of quadrilateral $EPON$, which are:

$$\begin{aligned}\begin{bmatrix}\dot{\theta}_1\\ \dot{\theta}_2\\ \dot{\theta}_3\end{bmatrix}&=\begin{bmatrix}\dfrac{h_1+m}{h_1(\frac{m\partial\varphi}{h_1\partial\theta_1}+1)} & \dfrac{-1}{\frac{m\partial\varphi}{h_1\partial\theta_1}+1} & \dfrac{-h_2}{(h_2+l_2)(\frac{m\partial\varphi}{h_1\partial\theta_1}+1)}\\ 0 & 1 & 0\\ 0 & 0 & 1\end{bmatrix}\begin{bmatrix}\dot{\gamma}_1\\ \dot{\theta}_2\\ \dot{\theta}_3\end{bmatrix}\\&=\boldsymbol{J}_\omega\begin{bmatrix}\dot{\gamma}_1\\ \dot{\theta}_2\\ \dot{\theta}_3\end{bmatrix}\end{aligned} \tag{12}$$

where h_1 is the length of EQ_1, h_2 is the length of FQ_2, m is the length of PE, and φ is the angle between PE and the horizontal line. These parameters can all be calculated based on geometric relationships.

With a view to simplify the calculation, an ideal grasping state of the mechanical finger is selected as the benchmark for optimization, as shown in Fig. 6(c). The rods a_1b_1, c_1b_1, a_2b_2, and b_2c_2 are perpendicular to each other, while ψ_1 and ψ_2 are set to135°. The lengths of each joint are set as l_1=63 mm, l_2=30 mm, and l_3=38 mm. The uniformity of force distribution of the finger in the ideal enveloping grasping state is adopted as the performance indicator. The following objective function f is defined as:

$$f=|f_1-f_2| \tag{13}$$

where

$$\begin{cases}f_1=\max(F_1,F_2,F_3)\\ f_2=\min(F_1,F_2,F_3)\end{cases} \tag{14}$$

Adding geometric constraints as:

$$\begin{cases}\delta_1=\varphi-\theta_1+\arcsin((a_1-c_1)/m)\\ \delta_2=\arcsin((a_2-c_2)/l_2)\\ \varphi_1=1.5\pi-\delta_1-\psi_1\\ \varphi_2=1.5\pi-\delta_2-\psi_2\\ b_1=\sqrt{m^2-(a_1-c_1)^2}\\ b_2=\sqrt{l_2^2-(a_2-c_2)^2}\end{cases} \tag{15}$$

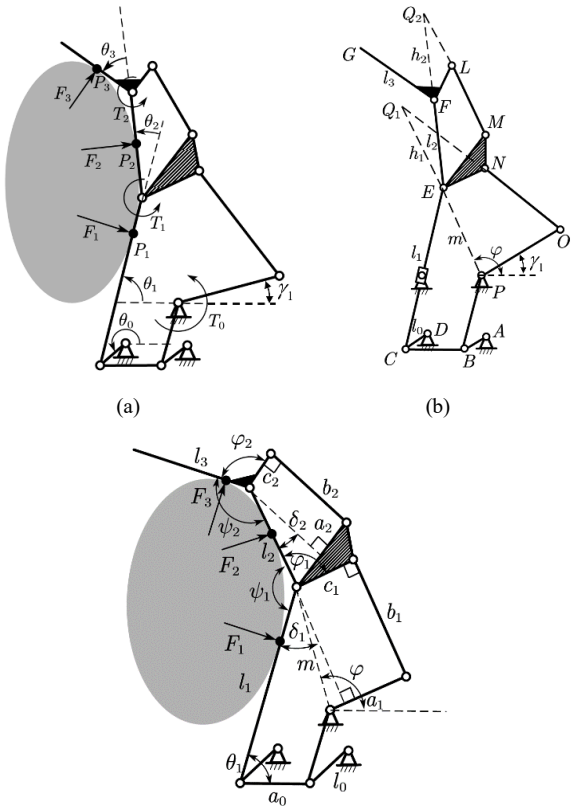

Fig. 6. Enveloping analysis of the finger. (a) Force analysis, (b) geometric parameter, (c) ideal state.

The variables including structural parameters a_0, a_1, a_2, c_1, c_2, and angle θ_1 are designated for optimization and then used to calculate h_1, h_2, m, φ. The driving torque T_0 of the finger is 1200 N·mm, and the forces generated by the torsion spring and joint friction are ignored. The value ranges for the optimized variables [a_0, a_1, a_2, c_1, c_2, θ_1] are set between the lower bounds [16, 22, 18, 12, 8, 40] and upper bounds [24, 28, 25, 24, 20, 70]. The genetic algorithm (GA) in the MATLAB optimization toolbox is employed for optimization with a population size of 5000, a stall generation of 50, and other parameters adopt default values. The termination condition of the program is that the weighted average change of the fitness function is less than 10^{-6}. After that, the rounded values of [a_0, a_1, a_2, c_1, c_2, θ_1] are [21mm, 25 mm, 24 mm, 20 mm, 15 mm, 59°] respectively. Thus, the forces on the three finger joints can be calculated as F_1=10.05 N, F_2=9.87 N, and F_3=9.74 N from (8)-(10).

III. Experimental Platform

We built a special experimental platform to fully test the performance of the designed manipulator, as shown in Fig. 7. It consists of a UR robotic arm, an underactuated manipulator, a power module, and a control system. The power provides 12V DC for drive module (L298N) of the linear motor (Stroke: 30mm, Thrust: 60N) and the servo motor (GDW RS0708-270°). The development board (Arduino mega2560) is used for controlling the linear motor and servo motor, as well as delivering the signals of the force sensor (FSR402) and angle sensor (SV01A103) to the computer in real time through serial port with 115200 baud rates.

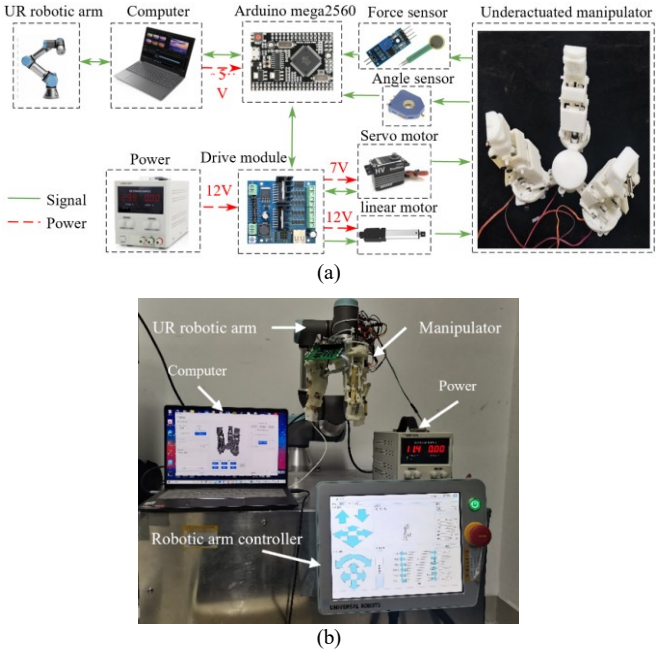

Fig. 7. Test platform for the manipulator. (a) Scheme of the control system, (b) experimental platform.

IV. Results and Discussion

A. Motion linearity of the fingertip

The method shown in Fig. 8 (a) was adopted for testing the linearity of the pinching motion of the fingertip. The laser displacement sensor was fixed to the fingertip to monitor its motion. The test was finished in 2.5 s, and the linear displacement was about 48mm. It can be seen from the trajectory curve is shown in Fig.8 (b) that within 2 seconds, the fingertip performs approximately line motion with a vertical displacement of about 0.3 mm and a quite low linear deviation of 0.63%. The deviation compared to 0.13mm (0.26%) in Fig. 5(b) mainly due to the accuracy of 3D printed parts and the unevenness of the workbench surface. From 2-2.5s, the vertical displacement of the fingertip increased rapidly because the fingertip can only move linearly within

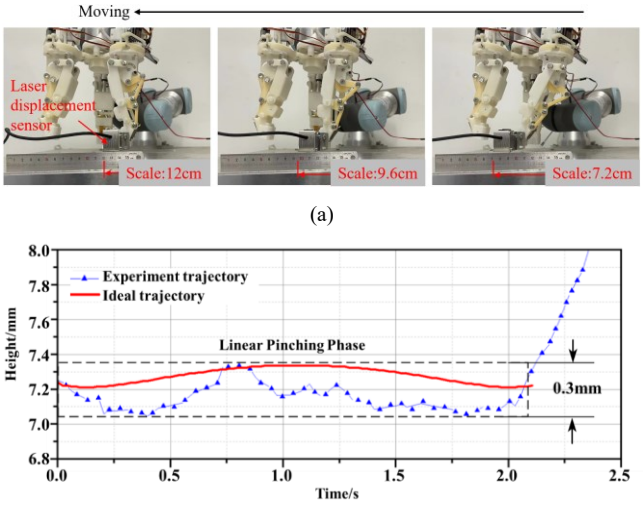

Fig. 8. The motion trajectory of mechanical finger. (a) Test method, (b) experimental result.

48mm range determined by the mechanical parameters. Beyond the linear motion range, the finger will perform an enveloping motion under the action of the constraint structure so that the height measured by the laser sensor will rise rapidly.

B. Contact force of the finger

To analyze the grasping ability of the developed manipulator, a test was conducted on the grasping force by using the FSR402 force sensor, as shown in Fig. 9(a) and (b). The finger was driven to envelope the cylinder-shaped sellotape, and the obtained contact force data is shown in Fig. 9(c). It can be found that during the process of enveloping, the PIP will first come into contact with the object, then followed by the MID, and finally the DIP. The process of releasing the object is the opposite. During the instantaneous touch and release of the object, there will be a sudden change in the contact force. This may be due to the momentary uneven force applied on the pressure sensor with the initial stage of grasping and unloading. In addition, during the process of enveloping, the maximum force applied to the PIP is about 9.3 N, the force on MIP is about 8.7 N, and the minimum force on the DIP is about 8.2 N. Due to the influence of unmodelled factors such as friction, the measured force is generally smaller than that of simulation and theoretical calculation (F_1=10.05 N, F_2 =9.87 N, F_3 =9.74 N). The contact forces on the three joints are similar to each other. This indicates that the force distribution on the finger joints is relatively uniform and consistent with the designing expectations.

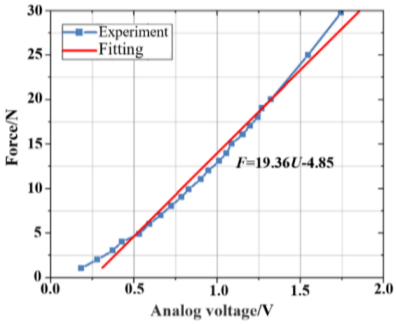

(a)

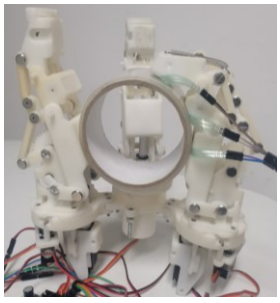

(b)

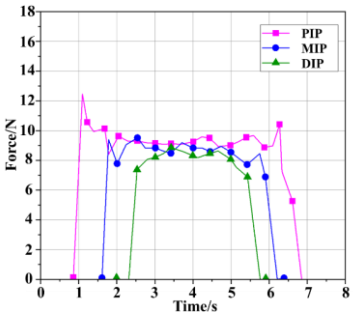

(c)

Fig. 9. The contact force test of mechanical finger. (a) The calibration of FSR402 force sensor, (b) experimental method, (c) experimental result.

C. Grasping ability of the manipulator

A grasping experiment was designed to demonstrate the capability of the proposed manipulator for grasping small and thin objects, and the target objects are a campus card with thickness of 0.9 mm, a sandpaper with thickness of 0.3 mm, and an M3 screw. The process of pinching can be divided into three steps: approaching the object, establishing a stable grasp, and lifting the object. as shown in Fig. 10. The robotic arm lowers the manipulator to make contact between the fingertips and the workbench. The experimental results show that the manipulator can grasp prescribed objects placed on the workbench without the need for additional displacement compensation by the robotic arm. This grasping function of manipulator relies on the pinching linkage mechanism proposed in this paper. Furthermore, the grasping experiments with pose-varied mode of manipulator were conducted to further verify the flexibility of the designed three-finger underactuated manipulator. As shown in Fig. 11, the target objects included sponge ball, screwdriver, cylinder-shaped sellotape, calculator, disinfectant spray bottle, and tea canister. For spherical objects, the designed manipulator can grasp the object from a flat surface with enveloping state. For other objects, it needs to be slightly raised for executing envelope grasp.

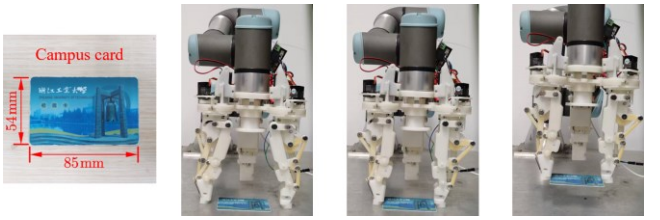

(a)

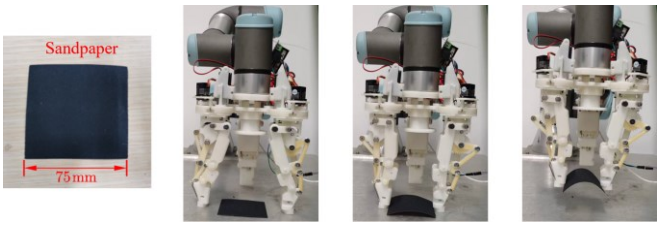

(b)

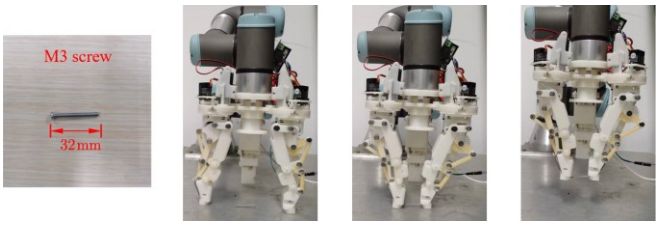

(c)

Fig. 10. Experiments of pinching small and thin objects. (a) Campus card with a thickness of 0.9 mm, (b) sandpaper with a thickness of 0.3 mm, (c) M3 screw.

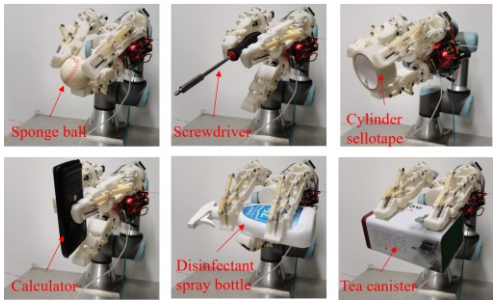

Fig. 11. Grasping objects with pose-varied mode of manipulator

D. Load capacity of the manipulator

The load capacity of the manipulator is an important indicator for evaluating its performance. As shown in Fig. 12, this test method employed the UR3 robotic arm to guide the manipulator to grasp a dumbbell with two 1.5 kg weights, and then lift it. As shown in Fig.12(b), the manipulator can grasp the dumbbell and maintain a stable state without falling. The experimental results demonstrate that the manipulator has a load capacity greater than 3 kg.

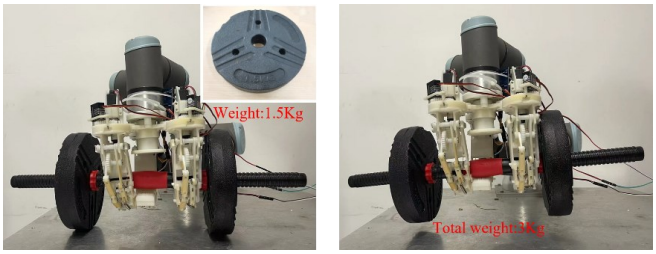

Fig. 12. Using the designed manipulator to grasp a dumbbell with two 1.5 kg weights.

V. Conclusion

This paper applies the inverted slider-crank line guiding mechanism to the structural of underactuated finger, and proposes a mechanical finger design scheme based on a multiple-linkage mechanism, which successfully makes the precise pinching and powerful grasping actions of the manipulator possible. Based on the geometric relationship of the linkage mechanism, the length configuration of the pinching linkage group is optimized to effectively reduce the trajectory error during the translational motion process, resulting in 0.26% for the line deviation. Furthermore, the structural parameters of the envelope linkage mechanism are optimized based on the uniformity of force distribution with the kinematic and contact force models of the underactuated finger, which is beneficial for the stability of grasping. The experimental results show that the designed manipulator has different grasping modes and a load capacity of more than 3 kg, which implies that it can adapt to grasping tasks of objects with different size, shape, and weight.

Acknowledgment

This work is financially supported by the Key Research and Development Program of Zhejiang (Grand No. 2021C04015), the Zhejiang Provincial Natural Science Foundation of China (Grand No. LZ23E050005).

References

[1] Bullock I M, Zheng J Z, Rosa S D L, et al. Grasp Frequency and Usage in Daily Household and Machine Shop Tasks[J]. IEEE Transactions on Haptics, 2013, 6(3): 296-308.

[2] M Grebenstein, M Chalon, G Hirzinger and R Siegwart. Antagonistically driven finger design for the anthropomorphic DLR Hand Arm System. 2010 10th IEEE-RAS International Conference on Humanoid Robots, Nashville, TN, USA, 2010, pp. 609-616, doi: 10.1109/ICHR.2010.5686342.

[3] S Phodapol, A Harnkhamen, N Asawalertsak, et al. Insect Tarsus-Inspired Compliant Robotic Gripper With Soft Adhesive Pads for Versatile and Stable Object Grasping. IEEE Robotics and Automation Letters, vol. 8, no. 5, pp. 2486-2493, May 2023, doi: 10.1109/LRA.2023.3251186.

[4] LI Shuang， MA Xiaojian，LIANG Hongzhuo，et al., "Vision-based Teleoperation of Shadow Dexterous Hand using End-to-End Deep Neural Network," 2019 International Conference on Robotics and Automation (ICRA), Montreal, Canada, 2019, pp. 416-422.

[5] Vertongen J, Kamper D G, Smit G, et al. Mechanical Aspects of Robot Hands, Active Hand Orthoses, and Prostheses: A Comparative Review. IEEE/ASME transactions on mechatronics, 2021,26(2):955-965.

[6] Daniel R. Ramírez Rebollo, Pedro Ponce and Arturo Molina. From 3 fingers to 5 fingers dexterous hands, Advanced Robotics, 31(2017)1051-1070.

[7] Liu, Hong, Ke Wu, Peter Meusel, Nikolaus Seitz, Gerd Hirzinger, M. H. Jin, Y. W. Liu, S. W. Fan, T. Lan, and Z. P. Chen. "Multisensory five-finger dexterous hand: The DLR/HIT Hand II." In IEEE/RSJ International Conference on Intelligent Robots and Systems (IROS), pp. 3692-3697. IEEE, 2008.

[8] Catalano M G, Grioli G, Farnioli E, et al. Adaptive synergies for the design and control of the Pisa/IIT SoftHand. The International Journal of Robotics Research, 2014, 33(5):768-782.

[9] S. Reza Kashef, Samane Amini, Alireza Akbarzadeh. Robotic hand: A review on linkage-driven finger mechanisms of prosthetic hands and evaluation of the performance criteria. Mechanism and Machine Theory, 145(2020)103677.

[10] Controzzi, Marco, Francesco Clemente, Diego Barone, Alessio Ghionzoli, and Christian Cipriani. "The SSSA-MyHand: a dexterous lightweight myoelectric hand prosthesis." IEEE Transactions on Neural Systems and Rehabilitation Engineering 25, no. 5 (2017): 459-468.

[11] Haoran L, Christopher J F, Matteo B, et al. BRL/Pisa/IIT SoftHand: A Low-Cost, 3D-Printed, Underactuated, Tendon-Driven Hand With Soft and Adaptive Synergies. IEEE Robotics and Automation Letters, vol. 7, no. 4, pp. 8745-8751, Oct. 2022, doi: 10.1109/LRA.2022.3187876.

[12] Ma, Raymond R., Lael U. Odhner, and Aaron M. Dollar. "A modular, open-source 3d printed underactuated hand." In Robotics and Automation (ICRA), 2013 IEEE International Conference on, pp. 2737-2743. IEEE, 2013.

[13] Xu, Zhe, and Emanuel Todorov. "Design of a highly biomimetic anthropomorphic robotic hand towards artificial limb regeneration." In International Conference on Robotics and Automation (ICRA), pp. 3485-3492. IEEE, 2016.

[14] D. Hidalgo-Carvajal, C. Herneth, A. Naceri and S. Haddadin, "End-to-End From Human Hand Synergies to Robot Hand Tendon Routing," in IEEE Robotics and Automation Letters, vol. 7, no. 4, pp. 10057-10064, Oct. 2022.

[15] Y. Cho, B. Kang, C. Park and J. Cheong, "Kinematics of Elastic Tendons for Tendon-Driven Manipulators With Transmission Friction," in IEEE/ASME Transactions on Mechatronics, vol. 27, no. 1, pp. 202-213, Feb. 2022.

[16] Y. Li, W. Lu, Y. Liu, D. Meng, X. Wang and B. Liang, "Optimization Design Method of Tendon-Sheath Transmission Path Under Curvature Constraint," in IEEE Transactions on Robotics, doi: 10.1109/TRO.2023.3255545.

[17] Gosselin C M. Adaptive robotic mechanical systems: A design paradigm[J]. JOURNAL OF MECHANICAL DESIGN, 2006, 128(1): 192-198.

[18] Belter JT, Segil JL, Dollar AM, Weir RF. Mechanical design and performance specifications of anthropomorphic prosthetic hands: A review. OURNAL OF REHABILITATION RESEARCH AND DEVELOPMENT, 2013, 50(5):599-617.

[19] Kim U, Jung D, Jeong H, et al. Integrated linkage-driven dexterous anthropomorphic robotic hand. Nat Commun 12, 7177 (2021).

[20] Kim EH, Lee SW, and Lee YK. A dexterous robot hand with a bio-mimetic mechanism. Int. J. Precis. Eng. Manuf. 12, 227–235 (2011).

[21] P. Wattanasiri, P. Tangpornprasert and C. Virulsri, "Design of Multi-Grip Patterns Prosthetic Hand With Single Actuator," in IEEE Transactions on Neural Systems and Rehabilitation Engineering, 2018, vol. 26, no. 6, pp. 1188-1198.

[22] Wu, L.; Kong, Y.; Li, X. Fully rotational joint underactuated finger mechanism and its kinematics analysis. J. Mech. Eng. 2017, 53, 47–54.

[23] Bégoc V, Krut S, Dombre E, et al. Mechanical design of a new pneumatically driven underactuated hand[C]//Proceedings 2007 IEEE International Conference on Robotics and Automation. IEEE, 2007: 927-933.

[24] Yamaguchi K, Hirata Y, Kosuge K. Underactuated robot hand for dual-arm manipulation[C]//2015 IEEE/RSJ International Conference on Intelligent Robots and Systems (IROS). IEEE, 2015: 2937-2942.

[25] Sun L, Zhang H, Lin H, et al. Design and Research of an Underactuated Manipulator Based on the Metamorphic Mechanism[J]. Sensors, 2022, 22(13): 4766.

[26] Luo C, Yang S, Zhang W, et al. MPJ hand: a self-adaptive underactuated hand with flexible fingers of multiple passive joints[C]//2016 international conference on advanced robotics and mechatronics (ICARM). IEEE, 2016: 184-189.

[27] Li J, Kong Y, Dong M, et al. Development of a linear-parallel and self-adaptive under-actuated hand compensated for the four-link and sliding base mechanism[J]. Robotica, 2022, 40(6): 2047-2064.

[28] Watanabe T, Morino K, Asama Y, et al. Variable-grasping-mode gripper with different finger structures for grasping small-sized items[J]. IEEE Robotics and Automation Letters, 2021, 6(3): 5673-5680.

[29] E. Zheng and W. Zhang, “An underactuated PASA finger capable of perfectly linear motion with compensatory displacement,” J. Mech. Robot. 11(1), 014505 (2019).

[30] Hamilton, R., Dunsmuir, R. A. Radiographic assessment of the relative lengths of the bones of the fingers of the human hand. Journal of Hand Surgery: British and European Volume, 2002, 27(6): 546-548.